Threshold law for ionization cross sections in the Temkin-Poet model

J. H. Macek
Department of Physics and Astronomy, University of Tennessee, Knoxville, Tennessee 37996-1501
and Oak Ridge National Laboratory, Post Office Box 2009, Oak Ridge, Tennessee 37831

W. Ihra
Department of Mathematics, Royal Holloway, University of London, Egham, Surry TW20 0EX, United Kingdom
(Received 14 June 1996; revised manuscript received 15 October 1996)

An integral representation of wave functions for the Temkin-Poet model of electron impact on atomic hydrogen is given. Approximate wave functions are evaluated analytically for large hyperradius to extract the ionization S-matrix element. An ionization cross section of the form $\exp[-aE^{-1/6}+bE^{1/6}]$, where a and b are positive constants, is derived. The exponential suppression of ionization for small E appears to be the quantum counterpart of the delayed onset of ionization in the classical theory for this model. [S1050-2947(97)03703-7]

PACS number(s): 34.80.−i

I. INTRODUCTION

Electron correlations are central to excitation and ionization of atoms by electrons and photons. A wave picture of dynamical correlations has been given by Fano [1], using insights derived from the classical Wannier theory [2], the semiclassical analysis of Rau [3] and Peterkop [4], and the adiabatic hyperspherical representation of Macek [5]. In Fano's picture, an outgoing Schrödinger wave in the hyperradius $R=\sqrt{r_1^2+r_2^2}$ emerges from the region where both electron coordinates r_1 and r_2 are of the order of 1 a.u. As it propagates to larger values of R, part of the wave branches off into waves concentrated in the potential valleys where $r_1 \ll r_2$ or $r_2 \ll r_1$. Waves concentrated in potential valleys represent excitation and the corresponding adiabatic states will be referred to as ''valley'' states [1]. A complimentary part of the wave localized in the region $r_1 \approx r_2$ continues to infinite distance and corresponds to ionization. This part propagates on the ridge of the potential and states concentrated here will be referred to as ''ridge'' states.

A complete theory must represent the dynamical evolution of both types of states, a task that has proved difficult for conventional atomic theory. Classical [2,6] and semiclassical methods [3,4,7] have been able to account for the asymptotic behavior of that part of the wave function which propagates on the ridge. Complete *ab initio* quantal calculations have not yet been able to reproduce the Wannier threshold law, although Crothers [8] has adapted the semiclassical wave functions of Peterkop [4] to conventional expressions for transition amplitudes and has computed absolute ionization cross sections near the threshold. This was the first calculation to obtain both the threshold law and the normalization constant. Rost [6] has solved the one-dimensional linear model, where $1/r_{12}$ is replaced by $1/(r_1+r_2)$, classically and obtained the energy variation of the cross section for total energy E between 0 and 0.4 a.u. The classical calculations did not obtain absolute cross sections, but the energy variation agrees well with the experiments of McGowan and Clarke [9]. Close-coupling calculations using a discrete basis [10,11] to represent the continuum have given accurate total cross sections for energies greater than 0.3 a.u. above the ionization threshold, but fail to obtain the Wannier threshold law. Hyperspherical close-coupling calculations using 100–300 channel functions [12] are consistent with the Wannier power law for $E>0.05$ a.u. These are the most complete calculations to date in the threshold region which employ well-established, but numerically intensive, methods. More basis states are apparently needed to push the calculations to still lower energy. It appears that completely *ab initio* methods will eventually succeed in reproducing the known cross sections in the Wannier threshold region. For photoionization of helium, Shakeshaft [13] has actually succeeded in obtaining the Wannier threshold law using a basis of outgoing-wave Sturmian functions.

None of the theories cited above incorporate Fano's picture of wave propagation. Direct solution of the Schrödinger equation in hyperspherical coordinates by Bohn [14] has yielded eigenphases which support the existence of a part of the wave that remains on the ridge, but cross sections for measurable processes were not obtained. Solution of the time-dependent Schrödinger equation using a wave-packet representation has proved feasible for energies of the order of 0.5 a.u. above threshold [15,16]. While the Wannier threshold law is not obtained, the wave function does appear to propagate in accord with Fano's picture. A surprising aspect of these calculations is that when the exact electron-electron interaction $V_{12}=1/|\mathbf{r}_1-\mathbf{r}_2|$ is replaced by the Temkin-Poet (TP) [17–20] model potential $V_{12}=1/r_>$, where $r_>$ is the larger of r_1 or r_2, the basic picture of wave propagation changes very little, yet it is expected that ''ridge'' states should play no role. In the TP model a threshold law appropriate for a product state of one Coulomb wave and a free-particle function, i.e., $\sigma \propto E^{1.5}$, is expected [18]. A further surprising result is that purely classical calculations [21] obtain ionization cross sections that vanish in the region $0<E<1/6$ a.u., even though ionization is energetically allowed. The quantal cross sections for the TP model differ considerably from the classical results and may correspond to a power law with a slightly lower exponent of 1.4 rather than 1.5 [15].

While the TP model employs a simplified electron-electron interaction, it plays an important role in an alterna-

tive picture of threshold ionization [19] which considers that ionization as well as excitation corresponds to waves propagating in the valleys where the two electron coordinates are not at all equal. It is also supposed that the electron velocities are quite different. In addition to the $1/r_>$ potential of the TP model, the faster electron also moves in the dipole potential of the nucleus and the slower electron. When the dipole potential is taken into account, a power law modified by an oscillating factor emerges.

Ionization cross sections for the TP model have been computed by three different groups using three quite different methods. Bray and Stelbovics [10] employ the convergent close coupling method, Meyer, Greene, and Bray [22] use the R-matrix method, and Ihra *et al.* [15] compute the time evolution of a Schrödinger wave. For energies above about 0.4 a.u., all of the cross sections agree within 10%. For lower energies in the threshold region, the three different methods disagree somewhat, especially with respect to the variation of the cross section with energy. This disagreement near threshold makes it difficult to determine if theories which emphasize wave propagation in the valleys of the potential represent viable alternatives to the Wannier theory in some energy range close to the threshold. The contradiction between classical and quantal theories remains unexplained, since there is apparently no quantal counterpart for the classical shift of the ionization onset.

The linear model also employs an approximate electron-electron interaction. The main difference between the models is that the linear model uses an approximate interaction consistent with propagation on the ridge, while the TP and dipole models employ potentials appropriate for propagation in the valleys. The purpose of the present manuscript is to derive a threshold law for the TP model using a recently developed theory [23,24] for systems whose total potential energy V is factorable in hyperspherical coordinates $V=RC(\Omega)$, where Ω is a set of hyperangles. The quantity $C(\Omega)$ will be referred to as the scaled potential. In parallel with the derivation for the TP model, the threshold law for the linear model will be obtained. It is known that the Wannier threshold law emerges in the linear model, and it will be verified that the theory of Ref. [24] obtains this result to within small corrections. Quantities referring to the linear model will be labeled with the subscript W and those referring to the Temkin-Poet model with the subscript TP.

A key feature of threshold laws is that they factor the cross section into a part that relates to wave motion in a region, called the reaction zone by Wannier, where all electron coordinates are small and a part that relates to a region, called the Coulomb zone, where the electron coordinates are large but the Coulomb potentials are still important. The factor that comes from the inner region is an analytic function of the total energy E but the factor that relates to the Coulomb zone is not. In the usual derivations of the Wannier threshold law this latter factor is simply a power of E. The method of Ref. [24] identifies this power of E as the first term in an asymptotic expansion of a function $s(E)$. Retention of more terms in the asymptotic expansion gives a threshold law which is more general than a power law and is often valid over a wider energy range than the simple power law. The function $s(E)$ has the dimensions of a cross section and differs from the absolute cross section only by a dimensionless, multiplicative analytic function $P_{\text{inner}}(E)$. The form of the function $s(E)$ is the main focus of this manuscript.

The theory of Ref. [24] is briefly reviewed in Sec. II. An expansion in angle-Sturmian eigenfunctions is a key feature of this theory. These eigenfunctions are defined by replacing the hyperradius R by an eigenvalue $\rho_j(\nu)$ in the equation defining adiabatic hyperspherical eigenfunctions, namely,

$$[\Lambda^2+\rho_j(\nu)2C(\Omega)]S_j(\nu;\Omega)=(\nu^2-1/4)S_j(\nu;\Omega), \tag{1.1}$$

where Λ^2 is the generalized angular momentum operator, ν is a parameter, $\rho_j(\nu)$ is the Sturmian eigenvalue, and $S_j(\nu;\Omega)$ the angle-Sturmian eigenfunction.

The angle-Sturmian functions are used to represent the kernel $\Phi(\nu,\Omega)$ in the Kontorovich-Lebedev transform [25] of the exact wave function

$$\Psi(R,\Omega)=\int_c \Phi(\nu,\Omega)R^{1/2}Z_\nu(KR)d(\nu^2/2). \tag{1.2}$$

The subscript c denotes a contour in the complex-ν plane chosen to fit boundary conditions, $Z_\nu(KR)$ is a Bessel function, and $K=\sqrt{2E}$. The coefficients in the expansion of $\Phi(\nu,\Omega)$ in the angle-Sturmian basis are determined by three-term recurrence relations which are solved approximately using the methods of Braun [26]. A relatively simple integral expression for the approximate wave function then emerges. The asymptotic form of this wave function is obtained and the approximate Jost matrix extracted.

The Jost matrix is used to compute the transition matrix elements. A notable feature of this theory is that, even though only one basis function is employed, an approximate value for every S-matrix element is obtained. In essence, the theory is complete at every level of approximation. At the lowest level of approximation employed here, indications are that the theory may be accurate to within 10% [24]. The lowest level approximate theory is known as the ''hidden crossing'' theory and was first developed in connection with ion-atom collisions by Solov'ev [27].

Fano's picture of wave propagation emerges naturally in this theory, but only the factoring of the potential plays a key role. The exact structure of the potential determines the details of the threshold law, but the emergence of a Wannier-type threshold law does not. It is therefore useful to see what threshold law emerges in the case of one-dimensional potentials such as the TP and linear models. In both cases the scaled potential $C(\Omega)$ is a function of only the hyperangle $\alpha=\arctan(r_2/r_1)$.

A single Sturmian is employed here so that $\Psi(R,\alpha)$ is approximated by

$$\Psi(R,\alpha)\approx\int_{-\infty}^{\infty}A(\nu)S(\nu;\alpha)R^{1/2}H_\nu^{(1)}(KR)d(\nu^2/2), \tag{1.3}$$

where

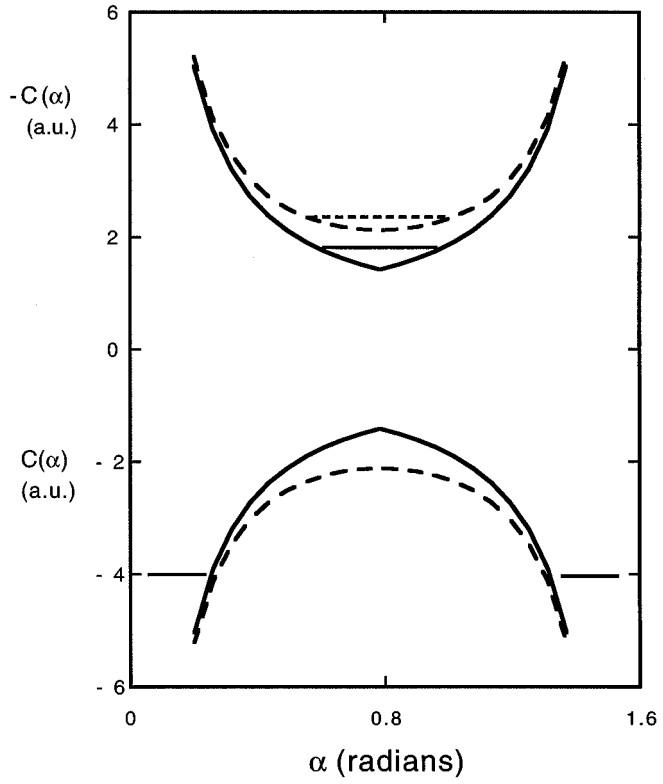

FIG. 1. Plot of the scaled potential $[\mathrm{sgn}(\rho)C(\alpha)]$ for positive ρ, lower figure, and for negative ρ, upper figure. The solid curve shows the scaled potential for the Temkin-Poet model, and the dashed curve for the linear model. The adiabatic energy eigenvalues for $|\rho|=8$ a.u. are indicated by horizontal lines. The lower figure illustrates the energy eigenvalue for a ''valley'' state and the upper figure illustrates the energy eigenvalue for a ''ridge'' state.

$$A[\nu(\rho)]=\frac{1}{\sqrt[4]{[2[E\rho(\nu)^2-\nu^2]}}\times\exp\left[i\int^{\nu(\rho)}\arcsin\left(\frac{\nu'}{\rho(\nu')}\right)d\nu'\right], \quad (1.4)$$

and an outgoing wave Bessel function $H_\nu^{(1)}(KR)$ is used. The subscript j on the eigenfunctions and eigenvalues is omitted since only one eigenfunction is employed.

We can easily see the role of valley and ridge states by considering the general properties of the Sturmian eigenvalues and eigenfunctions. The scaled potential $C(\alpha)$ is shown in the lower part of Fig. 1. For large negative ν^2, the eigenvalue ρ is approximately given by $\rho^2(\nu)\approx(\nu^2-1/4)/2\varepsilon_n$ where n is the principal quantum number of an electron bound in a one-electron state of the ion with binding energy ε_n. The corresponding Sturmian eigenfunction $S(\nu;\alpha)$ is just a one-electron hydrogenic radial function $P_n(\rho\alpha)$. It follows that the integral over negative ν^2 in Eq. (1.3) goes over a region where the Sturmian represents a valley state. The horizontal line in the valley region of Fig. 1(a) represents the product $\varepsilon\rho$ for $\rho=8$ and $n=1$. The wave functions for the valley states are essentially identical for the two potentials.

Alternatively, when ν^2 is large and positive, ρ must become negative. For negative ρ the potential term in Eq. (1.2) effectively changes sign as represented by the upper two scaled potential curves in Fig. 1(b). The bound states for negative ρ are concentrated in the region $\alpha\approx\pi/4$ and represent ridge states for both model potentials. The integral over positive ν^2 in Eq. (1.1) therefore goes over a region where the Sturmian eigenfunction represents a ridge state. A single angle-Sturmian function represents both valley and ridge motion and, for that reason, Eq. (1.1) accurately describes electron dynamics. Furthermore, it seems to be the most natural way to represent Fano's picture of electron correlations. As shown in Ref. [23], it gives a version of the Wannier threshold law where the Wannier index $\zeta_W=1.127$ is approximated by an ''adiabatic'' value $\zeta_W^{\mathrm{ad}}=1.104$.

To extract the threshold law it is necessary to compute the adiabatic energy eigenvalue $\varepsilon(\rho)$ for large negative ρ. The eigenvalue is computed in Sec. II. This eigenvalue is then used in the general cross section formula given in Ref. [24] to compute the threshold law. For the TP model we show in Sec. II that

$$\sigma\propto\exp[-aE^{-1/6}+bE^{1/6}], \quad a=6.87, \quad b=3.688, \quad (1.5)$$

a surprising expression, but one that may be in accord with the classical value of 0 for $E<1/6$ a.u. [21]. Note that exponentially vanishing probabilities often emerge in the quantum theory for processes that are classically forbidden.

The formula Eq. (1.5) can only be compared with more conventional calculations for this model. It has no experimental significance, but seems to indicate that Fano's picture of ionization via propagation on the ridge is to be traced to the factorization of the potential in hyperspherical coordinates, rather than to the detailed structure of $C(\alpha)$. The asymptotic function $s_{\mathrm{TP}}(E)$ is compared with the *ab initio* calculations of Refs. [10,15,22] in Sec. III.

II. REVIEW OF THE ANGLE-STURMIAN REPRESENTATION

In this section we briefly review the angle-Sturmian theory of Ref. [24] as it applies to the TP and linear models. The angle-Sturmian functions are defined as

$$\left[\frac{d^2}{d\alpha^2}-2\rho(\nu)C(\alpha)+\nu^2\right]S(\nu;\alpha)=0, \quad (2.1)$$

where ρ is an eigenvalue and ν is a parameter. For the TP model the scaled potential $C(\alpha)$ is given by

$$C(\alpha)=\begin{cases}-1/\sin(\alpha) & \text{if } \alpha<\pi/4\\ -1/\cos(\alpha) & \text{if } \alpha>\pi/4,\end{cases}$$

and for the linear model by

$$C(\alpha)=-\frac{1}{\sin(\alpha)}-\frac{1}{\cos(\alpha)}+\frac{1}{\sin(\alpha)+\cos(\alpha)}. \quad (2.2)$$

Because $C(\alpha)$ is negative definite, the Sturmian eigenvalues $\rho_n(\nu)$ and eigenfunctions are real for real ν^2 and are normalized according to

$$-\int_0^{\pi/2}S(\nu;\omega)^2C(\alpha)d\alpha=1. \quad (2.3)$$

The negative sign is used in Eq. (2.3) since $-C(\alpha)$ is positive definite.

The angle-Sturmian eigenfunctions $S(\nu;\alpha)$ and eigenvalues $\rho(\nu)$ relate to the more common adiabatic functions $\varphi(\rho;\alpha)$ and energy eigenvalues $\varepsilon(\rho)$ according to

$$2\varepsilon[\rho(\nu)]\rho(\nu)^2=\nu^2-1/4,$$

$$\varphi[\rho(\nu);\alpha]=NS(\nu;\alpha), \tag{2.4}$$

where

$$N=\sqrt{-\frac{\partial\rho(\nu)}{2\nu\partial\nu}}. \tag{2.5}$$

To compute ionization probabilities, the energy eigenvalues $\varepsilon(\rho)$ for large, negative ρ are needed. The computation of these quantities is carried out in Appendix A with the result

$$\varepsilon_{\mathrm{TP,asy}}(\rho)\approx\frac{C_{0,\mathrm{TP}}}{(-\rho)}+\frac{C'_{1,\mathrm{TP}}}{(-\rho)^{4/3}}+\frac{C_{2,\mathrm{TP}}}{(-\rho)^{5/3}}, \tag{2.6}$$

where

$$C_{0,\mathrm{TP}}=\sqrt{2},\quad C'_{1,\mathrm{TP}}=1.018\,81,\quad C_{2,\mathrm{TP}}=0.795\,37, \tag{2.7}$$

and where the subscript TP,asy indicates the asymptotic expression for the TP model. For the linear model one has the usual Wannier result [24]

$$\varepsilon_{W,\mathrm{asy}}(\rho)\approx\frac{C_{0,W}}{(-\rho)}+\frac{C_{1,W}}{(-\rho)^{3/2}}, \tag{2.8}$$

where now

$$C_{0,W}=3/\sqrt{2},\quad C_{1,W}=2^{-5/4}\sqrt{11}. \tag{2.9}$$

In both Eqs. (2.6) and (2.8) it must be remembered that $-\rho=\exp(-i\pi)\rho$ is a positive number. The branch of -1 is chosen so that $-\rho$ has a phase of 0 rather than 2π when $\rho=\exp(i\pi)|\rho|$.

For purposes of interpretation it is convenient to change variables from $\nu^2/2$ to ρ in Eq. (1.3). Substituting Eqs. (2.4) and (2.5) into Eq. (1.3) gives

$$\Psi(R,\Omega)=\int_{-\infty}^{\infty}B(\rho)\varphi(\rho,\alpha)R^{1/2}H^{(1)}_{\nu(\rho)}(KR)d\rho, \tag{2.10}$$

where an outgoing wave Bessel function is chosen and the coefficient $B(\rho)$ is

$$B(\rho)=\sqrt{-\frac{2\nu\partial\nu}{\partial\rho}}A[\nu(\rho)]. \tag{2.11}$$

III. DERIVATION OF THE THRESHOLD LAW

The integral in Eq. (2.10) is evaluated for large R using asymptotic approximations. For sufficiently large negative ρ less than some value $-\rho_Q$, $\varphi(\rho;\alpha)$ and $\nu(\rho)$ are replaced by their asymptotic values Eqs. (2.6) and (2.8),

$$\Psi(R,\Omega)\approx\int_{-\infty}^{-\rho_Q}B(\rho)\varphi_{\mathrm{asy}}(\rho;\alpha)R^{1/2}H^{(1)}_{\nu_{\mathrm{asy}}(\rho)}(KR)d\rho + \int_{-\rho_Q}^{\infty}B(\rho)\varphi(\rho;\alpha)R^{1/2}H^{(1)}_{\nu}(\rho)(KR)d\rho. \tag{3.1}$$

Both terms on the right-hand side are then evaluated in the stationary phase approximation and it is found [24] that both terms have points of stationary phase at $\rho=R$. For the second term, the functions $\varepsilon(\rho)$ and $\varphi(\rho;\alpha)$ are equal to the adiabatic quantities $\varepsilon_n(R)$ and $\varphi_n(R;\alpha)$, respectively, where the value of n specifies the branch of the function $\varepsilon_n(R)$. Different branches are reached by different paths of integration in the complex plane and the final result involves a sum over different paths. As shown in Ref. [24], this gives the amplitude for excitation of a particular bound state n.

In the first term, the function $\varphi_{\mathrm{asy}}(R;\alpha)$ at $\rho=R$ corresponds to the asymptotic function, defined for negative ρ in Eq. (A7), analytically continued to positive ρ. This function is real and exponentially damped for negative ρ but is complex and represents a wave that propagates outward from the ridge at $\alpha=\pi/4$ for positive R, as is seen most directly for the linear model where [24]

$$\varphi_{\mathrm{asy}}(\rho;\alpha)\approx\exp[-c\sqrt{-\rho}(\alpha-\pi/4)^2],\quad \rho<0,$$

$$\varphi_{\mathrm{asy}}(R;\alpha)\approx\exp[ic\sqrt{R}(\alpha-\pi/4)^2],\quad \rho=R>0. \tag{3.2}$$

It follows that the first term in Eq. (3.1) asymptotically describes the ionization component of the one-Sturmian wave function. Explicit evaluation of this component in the stationary phase approximation [24] gives the probability for ionization in the form

$$P(E)=P_{\mathrm{inner}}(E)P_{\mathrm{asy}}(E), \tag{3.3}$$

where

$$P_{\mathrm{inner}}(E)=\sum_{\mathrm{paths}}\exp\left[-2\,\mathrm{Im}\int_{\rho_0}^{\rho_Q}\sqrt{2[E-\varepsilon(\rho)-1/4\rho^2]} - \sqrt{2[E-\varepsilon_{\mathrm{asy}}(\rho)-1/4\rho^2]}d\rho\right], \tag{3.4}$$

$$P_{\mathrm{asy}}(E)=\exp[Q(E)], \tag{3.5}$$

$$Q(E)=-2\,\mathrm{Im}\int_{\rho_0}^{\infty}\sqrt{2[E-\varepsilon_{\mathrm{asy}}(\rho)-1/4\rho^2]}d\rho. \tag{3.6}$$

The constant ρ_0 is a real value of ρ on the branch of the function $\varepsilon(\rho)$ corresponding to the initial state. The sum over paths in Eq. (3.4) indicates that the amplitudes for all paths that connect ρ_Q and ρ_0 in the complex plane are summed coherently.

Both $P_{\mathrm{inner}}(E)$ and $P_{\mathrm{asy}}(E)$ depend upon ρ_0 but the product does not. For this reason the exact value is immaterial for the total cross section, although not for the factor $P_{\mathrm{asy}}(E)$ which is the main focus of the present work. The value of $\rho_0=4$ a.u. used here follows from consideration of where the angle-Sturmian function takes on characteristics of the

$n=2$ state near $\rho\approx 4$ a.u. The value of ρ_Q is only relevant to the calculation of $P_{\text{inner}}(E)$ and is not needed here. For completeness, it is nonetheless useful to note the ρ_Q is complex and large enough so that $P_{\text{inner}}(E)$ is insensitive to the exact value. The calculations of Ref. [24] use a value of $\rho_Q\approx 50\exp(i\pi/4)$, since terms of the order of $1/\rho^2$ are negligible at that point.

The quantity $P(E)$ gives the probability for populating the first ''ridge'' state whose asymptotic eigenvalue is shown in Fig. 1. The corresponding ionization cross section is

$$\frac{d\sigma(E)}{d\alpha_E}=P_{\text{inner}}(E)\frac{ds(E,\alpha_E)}{d\alpha_E}, \tag{3.7}$$

where

$$\frac{ds(E,\alpha_E)}{d\alpha_E}=\frac{\pi}{2E+1}|\varphi_{\text{asy}}(R_E,\alpha_E)|^2P_{\text{asy}}(E), \tag{3.8}$$

and the angle α_E is given in terms of the wave vectors k_1 and k_2 of the two electrons according to [28]

$$\alpha_E=\arctan(k_2/k_1). \tag{3.9}$$

The factor $P_{\text{inner}}(E)$ relates to electron motion in a region, called the reaction zone, where both electrons are close to the nucleus. Reference [23] computes this quantity with the exact electron-electron interaction. It could be computed using the same methods, but $P_{\text{inner}}(E)$ is not needed to extract threshold laws and will not be evaluated from first principles here. Values for this quantity do emerge in the next section by fitting the cross sections of Ref. [22] to the expression Eq. (3.7) integrated over relative electron energy.

Notice that, even though $\varepsilon_{\text{asy}}(\rho)$ and $\varphi_{\text{asy}}(\rho,\alpha)$ are real for negative ρ, they are complex for positive ρ. In contrast, $\varepsilon(\rho)$ and $\varphi(\rho,\alpha)$ are real for all ρ. For this reason the ionization channels only emerge when $\varepsilon(\rho)$ and $\varphi(\rho,\alpha)$ are first replaced by $\varepsilon_{\text{asy}}(\rho)$ and $\varphi_{\text{asy}}(\rho,\alpha)$ *before* the stationary phase approximation is employed. Presumably, they would also emerge when the integral is evaluated exactly or by alternative asymptotic approximations.

The quantity R_E is of the order of the Wannier radius C_0/E and is shown in Ref. [29] to be given by

$$R_E=4C_0/E \tag{3.10}$$

for the Wannier theory. Equation (3.10) will also be used for the TP model.

The magnitude of the asymptotic function $\varphi(R_E,\alpha_E)$ is independent of α_E for the linear model so that

$$|\varphi_{W,\text{ asy}}(R_E,\alpha_E)|^2=|N_W(R_E)|^2. \tag{3.11}$$

Equation (3.11) then predicts a flat distribution in α_E. Peterkop and Liepinsh [30] show that a more precise evaluation of the asymptotic function introduces a multiplicative factor of $\sin 2\alpha_E$ so that the distribution is actually flat in the energy E_1 of one electron [31]. This factor has not been verified for the TP model. The distribution for this model will be given as it emerges from the present theory, i.e., without the $\sin 2\alpha_E$ factor.

To compute the energy distribution for the TP model, it is necessary to analytically continue the asymptotic adiabatic function $\varphi_{\text{TP, asy}}(\rho,\alpha)$ from negative ρ to positive R_E. For large negative ρ, the eigenfunction $\varphi_{\text{TP, asy}}(\rho,\alpha)$ is concentrated in the classically allowed region near $\alpha=\pi/4$. For both the linear and the TP models, the classically allowed region becomes vanishingly small for large negative ρ, and the wave function in the classically forbidden region determines the relative electron energy distribution. In both the allowed and forbidden regions, the wave function for large ρ is given in terms of Airy functions $\text{Ai}(z)$ in Appendix A,

$$\varphi_{\text{TP,asy}}(\rho;\alpha)=N_{\text{TP}}(R_E)\text{Ai}(z_E-2\Delta), \tag{3.12}$$

where

$$z_E=\sqrt{2}[\exp(-i\pi)R_E]^{1/3}(\pi/4-\alpha) \tag{3.13}$$

and -2Δ is the first zero of $\text{Ai}'(z)$.

The distribution is integrated over α_E to obtain the total cross section. The integral is evaluated in Appendix B, with the result

$$\int_0^{\pi/2}|\varphi_{\text{TP,asy}}(R_E,\alpha_E)|^2d\alpha_E =\frac{|N_{\text{TP}}|^2}{2\pi\sqrt{6}\Delta R_E^{1/3}}\exp(2^{1/4}\sqrt{3\pi}\Delta R_E^{1/6}-2^{3/4}\sqrt{3/\pi}R_E^{-1/6}). \tag{3.14}$$

For comparison, the corresponding result for the linear model is

$$\int_0^{\pi/2}|\varphi_{W,\text{asy}}(R_E,\alpha_E)|^2\sin 2\alpha_E d\alpha_E=|N_W|^2. \tag{3.15}$$

The normalization constant for the linear model is known from Ref. [24] while the normalization constant for the TP model is derived in Appendix A. Substituting Eq. (3.10) into Eq. (A11) gives

$$|N(R_E)|^2=\begin{cases}\left(\dfrac{2C_{1,W}}{\pi}\right)^{1/2}R_E^{1/4}, & \text{linear model}\\ AR_E^{1/3}, & \text{TP model}\end{cases}$$

so that Eq. (3.14) becomes

$$\int_0^{\pi/2}|\varphi_{\text{TP,asy}}(R_E,\alpha_E)|^2d\alpha_E=\frac{A}{2\pi\sqrt{6}\Delta}\exp[2^{1/4}\sqrt{3\pi}\Delta R_E^{1/6} -2^{3/4}\sqrt{3/\pi}R_E^{-1/6}], \tag{3.16}$$

where $A=2.419$ is a constant.

The factor $P_{\text{asy}}(E)$ is computed using the approximation

$$\text{Im}\sqrt{2[E-\varepsilon(\rho)]}\approx-\frac{\text{Im}[\varepsilon_{\text{asy}}(\rho)]}{\sqrt{2[E+C_0/\rho]}}, \tag{3.17}$$

where

$$\mathrm{Im}\varepsilon(\rho)=\begin{cases} -C_{1,W}\rho^{-3/2}, & \text{linear model} \\ -\dfrac{\sqrt{3}}{2}[C_{1,\mathrm{TP}}\rho^{-4/3}+C_{2,\mathrm{TP}}\rho^{-5/3}], & \text{TP model} \end{cases} \tag{3.18}$$

for $\rho>0$. Terms of order $\varepsilon_{\mathrm{asy}}(R)^2$ are neglected. We have verified that these terms give only small corrections to $s_{\mathrm{TP}}(E)$ for $E>10^{-3}$ a.u.

These approximations are substituted into Eq. (3.6) and the integral over ρ evaluated using the identity

$$f(b,C_0,E)\equiv\int_{\rho_0}^{\infty}\frac{d\rho}{\rho^{b+1}\sqrt{2[E+C_0/\rho]}} =\frac{\rho_0^{-b}}{b\sqrt{2E}}{}_2F_1(1/2,b;b+1;-C_0/\rho_0E). \tag{3.19}$$

For $b=1/2$ the right-hand side of Eq. (3.19) diverges logarithmically as $E\to0$,

$$f(1/2,C_0,E)=\frac{2\rho_0^{-1/2}}{\sqrt{2E}}{}_2F_1(1/2,1/2;1/2+1;-C_0/\rho_0E) =\sqrt{\frac{2}{C_0}}\ln\left[\sqrt{\frac{C_0}{E\rho_0}}+\sqrt{1+\frac{C_0}{E\rho_0}}\right],\quad b=1/2 \tag{3.20}$$

but for $b<1/2$ it diverges as $E^{b-1/2}$ since

$$f(b,C_0,E)=\frac{\rho_0^{-b}}{b\sqrt{2E}}{}_2F_1(1/2,b;b+1;-C_0/\rho_0E) =\frac{\rho_0^{-b}}{\sqrt{2}(b-1/2)\sqrt{E+C_0/\rho_0}} \times{}_2F_1[1/2,1;3/2-b;E/(E+C_0/\rho_0)] +\frac{1}{\sqrt{2}}\frac{\Gamma(b)\Gamma(1/2-b)}{\Gamma(1/2)}C_0^{-b}E^{b-1/2}. \tag{3.21}$$

Substituting Eqs. (3.13)–(3.21) into the definition Eq. (3.6) of $Q(E)$, we get

$$Q_W(E)=C_{1,W}\sqrt{\frac{2}{C_{0,W}}}\left[\ln E-2\ln\left(\sqrt{\frac{C_{0,W}}{\rho_0}}+\sqrt{E+\frac{C_{0,W}}{\rho_0}}\right)\right] \tag{3.22}$$

for the linear model and

$$Q_{\mathrm{TP}}(E)=-\sqrt{3}[C_{1,\mathrm{TP}}f(1/3,C_{0,\mathrm{TP}},E)+C_{2,\mathrm{TP}}f(2/3,C_{0,\mathrm{TP}},E)] \tag{3.23}$$

for the TP model.

The results for the differential cross section function ds_W are

$$\frac{ds_W}{d\alpha_E}=\frac{2\pi}{2E+1}\sqrt{\frac{2C_{1,W}}{\pi}}C_{0,W}^{1/4}E^{-1/4}\exp[Q_W(E)]\sin2\alpha_E \tag{3.24}$$

in the linear model and

$$\frac{ds_{\mathrm{TP}}}{d\alpha_E}=\frac{A\pi}{2E+1}2^{5/6}E^{-1/3}\exp[Q_{\mathrm{TP}}(E)]|\mathrm{Ai}(z_E-2\Delta)|^2, \qquad z_E=2^{4/3}\exp[-i\pi/3]E^{-1/3}(\pi/4-\alpha_E) \tag{3.25}$$

in the TP model.

The integrated cross section functions are

$$s_W(E)=\frac{2\pi}{2E+1}\sqrt{\frac{2C_{1,W}}{\pi}}C_{0,W}^{1/4}E^{-1/4}\exp[Q_W(E)] \tag{3.26}$$

and

$$s_{\mathrm{TP}}(E)=\frac{A}{2E+1}\frac{1}{2\sqrt{6}\Delta}\exp[Q_{\mathrm{TP}}(E)] \times\exp(2^{2/3}\sqrt{3\pi}\Delta E^{-1/6}-2^{1/3}\sqrt{3/\pi}\Delta^2E^{1/6}). \tag{3.27}$$

In the limit as $E\to0$, the ionization cross sections in the two models become

$$\sigma_W=P_{\mathrm{inner}}(E)s_W(E)\propto E^{1.104}, \tag{3.28}$$

$$\sigma_{\mathrm{TP}}=P_{\mathrm{inner}}(E)s_{\mathrm{TP}}(E)\propto\exp[-6.870E^{-1/6}+3.680E^{1/6}], \tag{3.29}$$

where Eq. (3.16) has been used. When higher order terms in Eq. (3.17) are included, the coefficient of $E^{1/6}$ changes to 2.45.

It must be emphasized that the asymptotic expressions Eqs. (3.29) only give the ionization cross sections up to an undetermined, slowly varying, function $P_{\mathrm{inner}}(E)$. This is a feature of all threshold law theories, but present theory is unique in that an explicit expression Eq. (3.4) is given for this undetermined factor. Computation of this factor is not germane to the threshold law itself and is not attempted in this paper.

IV. RESULTS AND COMPARISONS WITH OTHER CALCULATIONS

The energy distribution for the TP model given by Eq. (3.25) is shown in Fig. 2 for three energies, namely $E=2$, 0.2, and 0.001 a.u. In all cases the distribution is nonuniform. The electrons concentrate in the valleys where one is faster than the other, as supposed at the outset. This tendency increases markedly as the energy decreases toward threshold.

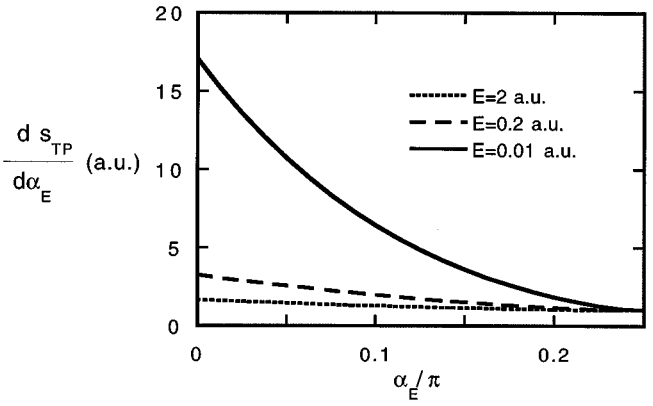

FIG. 2. Relative energy distribution of electrons from Eq. (3.25) for the TP model. The relative electron energy distributions for three energies $E=2$, 0.2, and 0.01 a.u. are shown. The distributions are normalized to unity at $\alpha_E=\pi/4$.

It must be emphasized that this distribution is uncertain owing to the possible presence of the factor $\sin 2\alpha_E$, which was deduced for the linear model on the basis of classical calculations [30]. Because there are no classical trajectories leading to ionization near $E\approx 0$, the methods of Ref. [30] cannot be used for this model. We can, however, compare with classical calculations for $E>0.17$ a.u.

The classical dynamics of the Temkin-Poet model have been studied in detail in Refs. [21,32]. We shall only give a brief outline here in order to understand how the classical energy distribution arises.

Classically, the onset of the total energy where both electrons can ionize is larger than the quantum mechanical threshold $E=0$. The ratio $E/|E_2|$ of the total energy to the absolute value of the energy of the initially bound electron must exceed a certain value β so that both electrons can ionize. The effect is most pronounced for $Z=1$ where β has the value 1/3. For helium, $Z=2$, $\beta=0.169\,777$. The classical onset of ionization is determined by this ratio only and not by the total energy E itself because the classical equations of motion can be scaled to an energy-independent form [21].

The finite threshold energy effect in the classical version of the Temkin-Poet model can be understood as follows: Let electron 1 be the incoming (outer) one ($r_1>r_2$) with positive energy, and let electron 2 be bound to the nucleus initially. The motion is separable as long as the electrons do not have equal distances r_1 and r_2 from the nucleus. Energy exchange between the two electrons only happens when an encounter on the diagonal $r_1=r_2$ takes place. In Ref. [21] it had been shown that, as a necessary condition for double escape, both electrons must have positive energy after the first encounter. It had also been shown that, if a second encounter takes place, the originally bound electron 2 will be rebound to the nucleus. In this case electron 1, which is now again the outer one, moves away rather rapidly from electron 2. A third encounter, which would be necessary for an energy exchange, is not possible and as a result only single ionization takes place. Double ionization can only happen if a trajectory stays in the region $r_2>r_1$ after the first encounter. This second necessary condition for double escape can only be fulfilled for $E/|E_2|>\beta$ [21].

To calculate classical properties from a representative set of trajectories, it is sufficient to characterize a set of initial conditions by two independent parameters [32]. One can be chosen to be the partitioning $E_1/|E_2|$ of the initial energies of the electrons. At given binding energy E_2 this determines the total energy. Another independent condition is given by the starting time: At the starting time the incoming electron 1 passes a fixed distance $r_1=d$ from the nucleus, while electron 2 performs bound oscillations in its radial coordinate r_2 (prior to the first encounter $r_1=r_2$). The starting time defines the asymptotic phase of the incoming electron with respect to the oscillatory motion of the bound electron. For the calculations, an equal distribution in the starting times for the set of trajectories is assumed.

Figures 3(a) and 3(b) present classical results taken from Ref. [32] for the electron distribution in the Temkin-Poet model for the case $Z=2$. To take the indistinguishability of the electrons into account only the smaller of the energies of the escaping electrons is recorded. The escape energy ϵ of the slower electron is measured in units of the total energy E thus ranging from 0 to 0.5 a.u. This interval is divided into

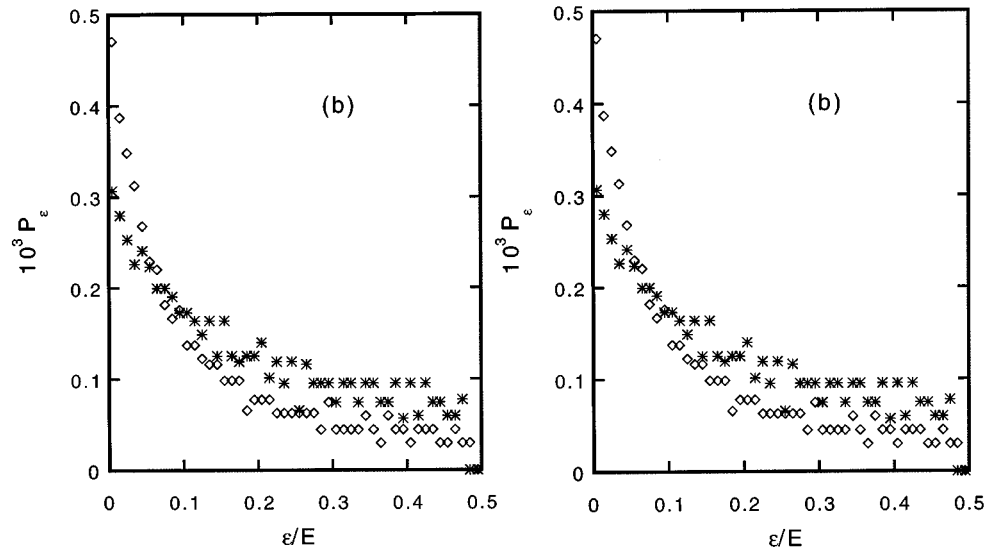

FIG. 3. Energy distribution probability P_ε of Ref. [21] for double escape near the classical threshold. The escape energy ε/E of the slower of both electrons is recorded and is measured in units of the total energy E. By taking the indistinguishability of the electrons into account, P_ε is symmetric with respect to $\varepsilon/E=0.5$. The energy distributions are plotted for different values of the ratio E/E_2 of the total energy to the absolute energy of the initially bound electron. (a) Asterisks: $E/|E_2|=0.2$, rhombi: $E/|E_2|=0.5$. (b) Asterisks: $E/|E_2|=5.0$, rhombi: $E/|E_2|=9.0$.

50 equally spaced parts, and for each partial interval the fraction of the total ionization probability is determined.

If the energy transfer from the incoming electron to the initially bound electron at the first encounter is not sufficiently large, a second encounter takes place and the electron will be rebound as described in the above scenario. Thus the electron which is the outer one after the first encounter must have at least a minimum fraction $\chi E (0<\chi<1)$ of the total energy E. The energy of the inner electron then is $E_{\rm in}=(1-\chi)E$. Close to the classical ionization threshold, χ is large and therefore $E_{\rm in}$ is small. Distributions with $E_{\rm in}>(1-\chi)E$ and thus symmetric energy distributions are not possible. Figure 3(a) shows that for $E/|E_2|=0.2$ and $E/|E_2|=0.5$, which is slightly above the classical ionization threshold $E/|E_2|=0.169\,77$, the energy distribution is approximately constant from $\epsilon/E=0$ to its maximum allowed value $E_{\rm in}$. There it drops to zero abruptly. This is in strong contrast to the behavior of the classical energy distribution in the collinear model for energies near threshold where a flat distribution with a slight maximum at equal energy $\epsilon/E=0.5$ is observed [6]. At higher energies of the incoming electron Fig. 3(b) shows that a maximum appears at the completely unsymmetric energy distribution $\epsilon/E=0$, which becomes more pronounced as the energy of the incoming electron increases.

Although the classical energy distributions were calculated for $e^-+\mathrm{He}^+$, i.e., $Z=2$, the results for $Z=1$ are expected to be quite similar, the only difference being the higher classical ionization threshold. The preferred unequal sharing of energy near the threshold in the Temkin-Poet model seems to be the classical counterpart of the quantum mechanical result which also prefers an unequal sharing. The main difference is that the energy distribution function in the quantum mechanical case is still a smooth function in the hyperangle α_E or ϵ/E, respectively, contrary to the abrupt drop to zero in the classical case.

The classical relative energy distributions are proportional to

$$\frac{d\sigma}{d\varepsilon_2}=\frac{d\sigma}{d\alpha_e}\frac{1}{\sin 2\alpha_a} \tag{4.1}$$

since $\varepsilon_2=E\sin^2\alpha_e$ asymptotically [28]. Equation (4.1), together with the quantal distributions of Fig. 2, show that the quantal energy distributions differential in $d\varepsilon_2$ are singular at $\alpha_e=0$, whereas the classical results are not. This suggests that the approximate quantal distributions are incorrect near $\alpha_e=0$, as they are in the conventional Wannier theory [30]. For E sufficiently above the classical threshold, it appears that the correct quantal distribution should incorporate a factor of $\sin 2\alpha_e$. For energies below the classical threshold, it is necessary to employ a more accurate asymptotic representation of the Sturmian functions for positive ν, and possibly to employ more than one Sturmian in the representation of Eq. (1.3) to obtain this factor. These improvements are not expected to affect the exponential factors in Eq. (3.5) significantly, but could introduce a more complicated energy dependence in Eq. (3.16).

The total ionization cross section functions $s(E)$ for the two models are compared over an extended energy range of 1 a.u. in Fig. 4. The two cross sections differ by a factor of 2

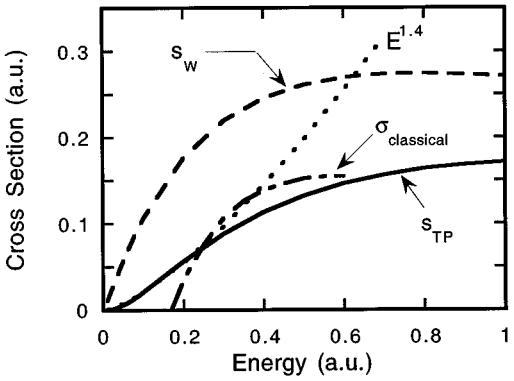

FIG. 4. Comparison of threshold ionization cross sections. The solid curve is the asymptotic cross section function $s_{\rm TP}(E)$ of Eq. (3.25) for the Temkin-Poet model, the dashed curve is $s_W(E)$ of Eq. (3.24) for the linear model, the dotted curve uses $E^{1.4}$ for the ionization probability, and the dot-dashed curve is the classical cross section of Ref. [21].

over most of the energy range, but they differ substantially in shape only between $0<E<0.1$ a.u., where ionization in the TP model is dramatically suppressed. This suppression may be the quantal counterpart of the vanishing classical cross section between $0<E<0.167$ a.u. Also shown is the classical cross section in the TP model. It departs significantly from $s_{\rm TP}(E)$, indicating that classical calculations are unreliable near the threshold for ionization.

The classical cross section in the linear model is not known absolutely, but Ref. [6] reports normalized classical cross sections over a 0.3 a.u. energy range. The ratio of the classical cross section of Ref. [6] to $s_{\rm W}(E)$ for the linear model is shown in Fig. 5. The ratio never departs from unity by more than 5%. For this model the classical and asymptotic quantal cross sections agree very well. The good agreement with the asymptotic quantal cross section indicates that the classical calculation succeeds because most of the energy variation comes from the statistical factor $(2E+1)^{-1}$ and $P_{\rm asy}(E)$. The latter factor pertains only to a region where the potential is well approximated by a harmonic oscillator potential, and it is known that classical and quantal results for such potentials are often nearly identical. In general, how-

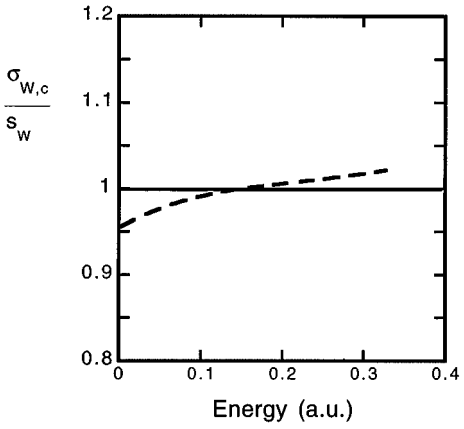

FIG. 5. Ratio of the classical cross sections of Ref. [6] for the linear model to $s_W(E)$ vs energy. The ratio has been normalized to unity at $E=0.15$ a.u.

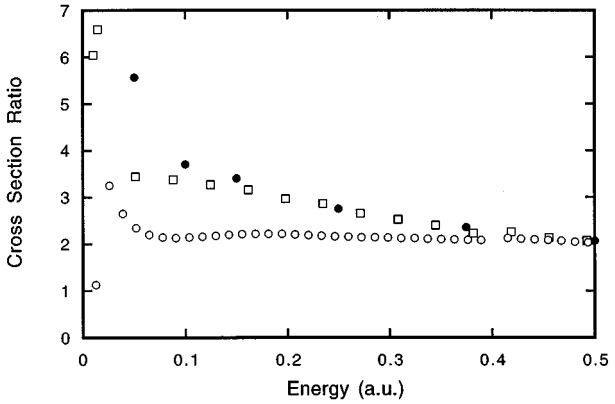

FIG. 6. Comparison of the ratio of computed cross sections $\sigma(E)$ to the asymptotic cross section functions $s_{\mathrm{TP}}(E)$ vs E. The solid circles employ cross sections of Ref. [15] computed using the time-dependent method, open squares employ the convergent close coupling results of Ref. [10], and the open circles use the R-matrix results of Ref. [22].

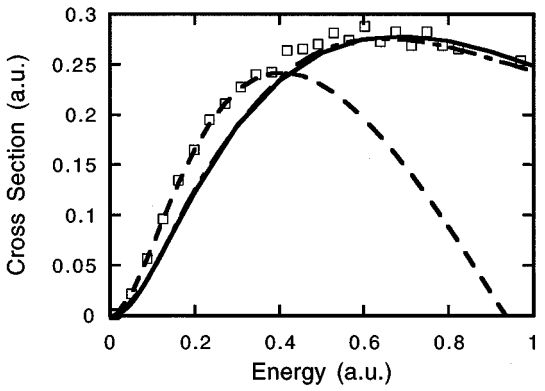

FIG. 7. Plot of the fitted cross sections $P_{\mathrm{inner}}(E)s_{\mathrm{TP}}(E)$ vs E. The data are as in Fig. 6, the dashed curve is the fit to the convergent close coupling cross section, and the solid curve is the fit to the R-matrix calculations.

ever, classical calculations are unreliable near threshold, but do agree when the potential for negative ρ has the harmonic oscillator form.

The quantal cross section that we obtain can only be tested by comparing with other calculations. Ihra *et al.* [15] have fitted quantal cross sections for the TP model in the threshold region to an $E^{1.4}$ power law. While it is clear that this power law cannot match the expression that we obtain in the region $0<E<0.04$, it may fit at higher energies. If we fit the cross section between $0.1<E<0.2$ a.u. to a power law, we find a power of 1.44, but a fit to the cross section in the range $0.1<E<0.3$ gives 1.39. It seems that a power of 1.4 agrees reasonably well in the latter range, as shown by the dotted curve in Fig. 4.

Since the asymptotic function $s(E)$ is determined by the region of intermediate and large R, it only gives the cross section up to a multiplicative, slowly varying function $P_{\mathrm{inner}}(E)$,

$$\sigma(E)=P_{\mathrm{inner}}(E)s(E). \tag{4.2}$$

To compare the present theory with available *ab initio* calculations of Refs. [10,15,22] we plot the ratio $\sigma(E)/s(E)$ vs E in Fig. 6.

For the time-dependent calculations the ratio is linear in E over the range 0.1 a.u. $<E<0.25$ a.u., but there are only three points in this range so a fit to this cross section does not test the threshold law. In addition, the lowest energy point at $E=0.05$ a.u. is outside of a fit to a linear function.

The convergent close coupling ratio is linear over the wider energy range 0.05 a.u.$<E<0.35$ a.u., and includes nine computed points. Only the two lowest points very close to threshold are outside a linear fit. For this cross section the fitted function $P_{\mathrm{inner}}(E)$ is found to be

$$P_{\mathrm{inner,\,CCC}}(E)=3.75\times(1-1.07\times E),$$

$$0.05\text{ a.u.}<E<0.35\text{ a.u.} \tag{4.3}$$

The R-matrix ratio is also a linear function down to an energy of the order of 0.08 a.u., which is somewhat higher than for the convergent close coupling ratio. Alternatively, this ratio is linear up to a much higher energy and includes many more computed points. We find that the fit

$$P_{\mathrm{inner},R}(E)=2.4\times(1-0.33\times E) \tag{4.4}$$

holds within a few percent up to the surprisingly high energy of 1.5 a.u.

The fitted and computed cross sections are compared in Fig. 7. Except for the lowest energy points, where *ab initio* methods would have difficulty computing the exponentially small cross sections that we predict, the available data are in agreement with our threshold law over an energy range of the order of 0.3 a.u. Better agreement with a threshold law cannot be expected, however we note that such better agreement emerges for the R-matrix calculations. Here the fit is seen to be excellent over a 1.0 a.u. energy range. Furthermore, both the normalization constant and the coefficient of the linear term are much smaller for this cross section than for the other two, indicating a significant difference between the *ab initio* calculations. Our analytic threshold law favors the R-matrix calculations, but is consistent with all calculations except for the lowest energy points.

A slow variation of $P_{\mathrm{inner},R}(E)$ with E is expected near threshold, but a rapid variation is seen in Fig. 6, most likely because the R-matrix calculations are not well-adapted to the threshold region. It is also possible that our asymptotic representation of the integrated cross section is in error owing to uncertainties in the relative energy distributions. Even so, the ratio never varies by more than 75%.

It is also possible that any reasonable function $s(E)$ might show similar agreement. To demonstrate that this is not the case, the ratio (not shown) of $\sigma_R(E)$ to $s_W(E)$ was computed and found to vary by a factor or 15 between $E=0$ and 0.08 a.u., and by a factor of 3 between $E=0.08$ and 0.5 a.u. On this basis it is apparent that the good agreement seen in Fig. 7 is not accidental.

It must be emphasized that the good agreement over the extended energy range tests the complete function $s_{\mathrm{TP}}(E)$ of Eq. (3.27) and not just the threshold law given by Eq. (3.29). The good agreement with the R-matrix calculations suggests that the complete expression Eq. (3.27) accurately represents effects of electron motion in the Coulomb zone.

The slow variation of $P_{\mathrm{inner},R}(E)$ seen in Fig. 6 over an extended energy range suggests that the ''top-of-barrier'' mechanism responsible for the standard Wannier threshold law also operates for the simple Temkin-Poet model. This mechanism is not identified in any of the reported calculations, but the eigenphase method of Ref. [14] could provide independent evidence for Fano's picture of wave propagation that emerges from our derivation of $\sigma_{\mathrm{TP,asy}}$. If our surmise that ionization proceeds via wave propagation on the ridge is correct, then an eigenphase characteristic of such motion should be evident for the TP model as it is for the real two-electron interaction [14].

Note added. Klaus Bartschat has informed us that recent CCC and R-matrix calculations [33] for this model obtain more reliable cross sections between 0.1 and 1 eV above the ionization threshold. Except for the point at 0.1 eV, the new R-matrix calculations agree well with our analytic expression.

ACKNOWLEDGMENTS

This research is sponsored by the Division of Chemical Sciences, U.S. Department of Energy, under Contract No. DE-AC05-960R22464 managed by Lockheed-Martin Energy Research Corporation. Support for one of us (J.H.M.) by the National Science Foundation under Grant No. PHY-9222489 is gratefully acknowledged. We also wish to thank J. M. Rost and K. W. Meyer for giving us tables of their published data. W.I. would like to thank H. Friedrich and P. O'Mahony for fruitful discussions and G. Handke for providing us with his data. Financial support for W.I. by the EU Human Capital and Mobility Program under Contract No. CT930350 is gratefully acknowledged. J.H.M. also thanks Colm Whelan for valuable discussions and for travel support under NATO Grant No. CRG.950407.

APPENDIX A: ASYMPTOTIC EIGENVALUES AND EIGENFUNCTIONS FOR THE TEMKIN-POET MODEL

The adiabatic eigenvalues are solutions of

$$\left[-\frac{1}{2\rho^2}\frac{d^2}{d\alpha^2}-\frac{1}{\rho}C(\alpha)-\varepsilon(\rho)-\frac{1/4}{\rho^2}\right]\varphi(\alpha)=0, \quad \text{(A1)}$$

where

$$C(\alpha)=\frac{1}{\sin\alpha}, \quad \alpha<\pi/4,$$

$$C(\alpha)=\frac{1}{\cos\alpha}, \quad \alpha>\pi/4 \quad \text{(A2)}$$

with the boundary conditions

$$\left.\frac{d\varphi}{d\alpha}\right|_{\alpha=\pi/4}=0 \quad \text{(A3)}$$

for spin zero states. We will solve this equation for negative ρ to find the eigenvalues pertinent to ionization.

Expanding $C(\alpha)$ about $\alpha=\pi/4$, introducing the variable $x=\pi/4-\alpha$, and defining $\Delta_{\mathrm{TP}}(\rho)$ according to

$$\varepsilon(\rho)=\sqrt{\frac{2}{(-\rho)}}+2\frac{\Delta_{\mathrm{TP}}(\rho)}{(-\rho)^{4/3}}-\frac{1/4}{\rho^2} \quad \text{(A4)}$$

gives

$$\left[\frac{d^2}{dx^2}-2\sqrt{2}(-\rho)\left(x+\frac{3}{2}x^2\right)+4\Delta_{\mathrm{TP}}(\rho)(-\rho)^{2/3}\right]\varphi=0, \quad x>0. \quad \text{(A5)}$$

The variable x is scaled according to

$$z=8^{1/6}(-\rho)^{1/3}x=\sqrt{2}(-\rho)^{1/3}x, \quad \text{(A6)}$$

so that the Schrödinger equation becomes

$$\left[\frac{d^2}{dz^2}-z-\frac{3}{2\sqrt{2}(-\rho)^{1/3}}z^2+2\Delta_{\mathrm{TP}}(\rho)\right]\varphi=0, \quad z>0. \quad \text{(A7)}$$

For sufficiently large $(-\rho)$ the quadratic potential term is neglected, in first approximation and $\Delta_{\mathrm{TP}}(\rho)\approx\Delta$, where Δ is independent of ρ. Then Eq. (A7) becomes a differential equation for the Airy function $\mathrm{Ai}(z-2\Delta)$ and the eigenvalue is determined by the requirement that the derivative of the function vanishes at $z=0$;

$$\mathrm{Ai}'(-2\Delta)=0. \quad \text{(A8)}$$

Numerical solution of this equation for the first zero of $\mathrm{Ai}'(-2\Delta)$ gives $2\Delta=1.0188$. The adiabatic wave function $\varphi_{\mathrm{TP,asy}}(R;\alpha)$ is then given by

$$\varphi_{\mathrm{TP,asy}}(\rho;\alpha)=N(\rho)\mathrm{Ai}(z-2\Delta). \quad \text{(A9)}$$

The normalization integral is evaluated numerically for $\rho\pi/4\rightarrow\infty$ with the result

$$\int_0^\infty \mathrm{Ai}(z-2\Delta)^2dz=0.292\ 322 \quad \text{(A10)}$$

so that the square of the normalization constant is given by

$$N^2(\rho)=A(-\rho)^{1/3}, \quad \text{(A11)}$$

where $A=1/0.292\ 322\sqrt{2}=\ 2.419\ 00$.

The contribution of the x^2 term in Eq. (A5) to $\Delta_{\mathrm{TP}}(\rho)$ is computed in first order perturbation theory. The expectation value of x^2 is

$$\langle x^2\rangle=2\int_0^\infty N^2\mathrm{Ai}^2(z-2\Delta)x^2dx$$

$$=\frac{2N^2}{2\sqrt{2}(-\rho)}\int_0^\infty \mathrm{Ai}^2(z-2\Delta)z^2dz=\frac{N^2}{\sqrt{2}(-\rho)}0.219\ 21, \quad \text{(A12)}$$

where the last line follows from direct numerical evaluation of the integral,

$$\int_0^\infty \mathrm{Ai}(z-2\Delta)^2z^2dz=0.219\ 207. \quad \text{(A13)}$$

We then have

$$2\Delta_{\mathrm{TP}}(\rho)=1.0188+\frac{3}{4(-\rho)^{2/3}}2\sqrt{2}(-\rho)\frac{N^2}{\sqrt{2}(-\rho)}0.219\ 27 \tag{A14}$$

$$=1.0188+\frac{3}{2(-\rho)^{1/3}}0.219\ 21A=1.0188+\frac{0.795\ 37}{(-\rho)^{1/3}}. \tag{A15}$$

Substituting this result into the expression for $\varepsilon_{\mathrm{TP,asy}}(\rho)$ gives

$$\varepsilon_{\mathrm{TP,asy}}(\rho)=\frac{C_{0,\mathrm{TP}}}{-\rho}+\frac{C'_{1,\mathrm{TP}}}{(-\rho)^{4/3}}+\frac{C_{2,\mathrm{TP}}}{(-\rho)^{5/3}}, \tag{A16}$$

where

$$C_{0,\mathrm{TP}}=\sqrt{2},\quad C'_{1,\mathrm{TP}}=1.0188,\quad C_{2,\mathrm{TP}}=0.795\ 37. \tag{A17}$$

APPENDIX B: EVALUATION OF AN INTEGRAL

The differential equation for $\mathrm{Ai}(z-2\Delta)$, where $z=xe^{-i\pi/3}$, with x and Δ real, can be written

$$\left[\frac{d^2}{dx^2}+x+2\Delta e^{-i2\pi/3}\right]\mathrm{Ai}=0. \tag{B1}$$

Using this equation for Ai and its complex conjugate, one has from Green's theorem that

$$e^{-i\pi/3}\mathrm{Ai}^*\mathrm{Ai}'-e^{i\pi/3}\mathrm{Ai}\mathrm{Ai}'^*+2\Delta(e^{-2i\pi/3}-e^{2i\pi/3})\int|\mathrm{Ai}|^2dx=0. \tag{B2}$$

Equation (B2) holds as an indefinite integral. For $x=\sqrt{2}R_E^{1/3}(\pi/4-\alpha_E)$ with the integration range $0<\alpha_E<\pi/4$, and using $\mathrm{Ai}'(-2\Delta)=0$, we have from the above equation the result

$$[e^{-i\pi/3}\mathrm{Ai}(X)^*\mathrm{Ai}'(X)-e^{i\pi/3}\mathrm{Ai}(X)\mathrm{Ai}'(X)^*]-4\Delta i\ \sin(2\pi/3)\sqrt{2}R_E^{1/3}\int_0^{\pi/4}|\mathrm{Ai}|^2d\alpha_E=0, \tag{B3}$$

where the Airy functions are evaluated at $X=X_0-2\Delta$ with $X_0=\sqrt{2}e^{i\pi/3}R_E^{1/3}\pi/4$.

For large values of R_E we may use the asymptotic forms of the Airy functions in the surface term. With the neglect of a small correction of the order of $\Delta/(2R_E^{1/3})$, we have from Eqs. (10.4.59) and (10.4.61) of Ref. [34] the result

$$\frac{1}{2\pi}\exp[-\zeta_E-\zeta_E^*]-2\Delta\sqrt{6}R_E^{1/3}\int_0^{\pi/4}|\mathrm{Ai}|^2d\alpha_E=0, \tag{B4}$$

where

$$\zeta_E=\frac{2}{3}(X_0-2\Delta)^{3/2}. \tag{B5}$$

This expression is then used to write the integral over $|\varphi_{\mathrm{TP,asy}}(R_E,\alpha_E)|^2$ as

$$\int_0^{\pi/2}|\varphi_{\mathrm{TP,asy}}|^2d\alpha_E=2\int_0^{\pi/4}|\varphi_{\mathrm{TP,asy}}|^2d\alpha_E=\frac{A}{2\pi\sqrt{6}\Delta}\exp(-\zeta_E-\zeta_E^*). \tag{B6}$$

For $X_0\gg\Delta$ we may expand ζ_E in powers of the small quantity Δ/X_0 to obtain

$$\zeta_E+\zeta_E^*\approx-2\Delta(X_0^{1/2}+X_0^{*1/2})+\Delta^2(X_0^{-1/2}+X_0^{*-1/2})=-2^{2/3}\sqrt{3\pi}\Delta E^{-1/6}+2^{1/3}\sqrt{3/\pi}\Delta^2E^{1/6}. \tag{B7}$$

This gives the desired expression

$$2\int_0^{\pi/4}|\varphi_{\mathrm{TP,asy}}|^2d\alpha_E=\frac{A}{i\sqrt{6}\Delta}[e^{-i\pi/3}\mathrm{Ai}(X)^*\mathrm{Ai}'(X)-e^{i\pi/3}\mathrm{Ai}(X)\mathrm{Ai}'(X)^*]\approx\frac{A}{2\pi\sqrt{6}\Delta}\exp(2^{2/3}\sqrt{3\pi}\Delta E^{-1/6}-2^{1/3}\sqrt{3/\pi}\Delta^2E^{1/6}). \tag{B8}$$

[1] U. Fano, Rep. Prog. Phys. **46**, 97 (1983).
[2] G. H. Wannier, Phys. Rev. **90**, 817 (1953).
[3] A. R. P. Rau, Phys. Rev. A **4**, 207 (1971).
[4] R. Peterkop, J. Phys. B **4**, 513 (1971).
[5] J. H. Macek, J. Phys. B **1**, 831 (1968); C. D. Lin, Rep. Prog. Phys. **257**, 1 (1995).
[6] J. M. Rost, Phys. Rev. Lett. **72**, 1998 (1994).
[7] J. M. Feagin, J. Phys. B **17**, 2433 (1984).
[8] D. S. Crothers, J. Phys. B **19**, 463 (1986).
[9] J. W. McGowan and E. M. Clarke, Phys. Rev. **167**, 43 (1968).
[10] I. Bray and A. T. Stelbovics, Phys. Rev. Lett. **70**, 746 (1993); At. Data Nucl. Data Tables **58**, 67 (1994).
[11] Y. D. Wang and J. Callaway, Phys. Rev. A **50**, 2327 (1994).
[12] D. Kato and S. Watanabe, Phys. Rev. Lett. **74**, 2443 (1995).
[13] R. Shakeshaft (private communication).
[14] J. Bohn, Phys. Rev. A **51**, 1110 (1995).
[15] W. Ihra, M. Draeger, G. Handke, and H. Friedrich, Phys. Rev. A **52**, 3752 (1995).
[16] M. S. Pindzola and D. R. Schultz, Phys. Rev. A **53**, 1525 (1996).
[17] A. Temkin, Phys. Rev. **126**, 130 (1962).
[18] A. Temkin, Phys. Rev. Lett. **16**, 835 (1966).
[19] A. Temkin, Phys. Rev. Lett. **49**, 365 (1982); M. K. Srivastova and A. Temkin, Phys. Rev. A **43**, 3570 (1991).

[20] R. Poet, J. Phys. B **11**, 3081 (1978); **13**, 2995 (1980); **14**, 91 (1981).
[21] G. Handke, M. Draeger, W. Ihra, and H. Friedrich, Phys. Rev. A **48**, 3699 (1993).
[22] K. W. Meyer, C. H. Greene, and I. Bray, Phys. Rev. A **52**, 1334 (1995).
[23] J. H. Macek, S. Yu Ovchinnikov, and S. V. Pasovets, Phys. Rev. Lett. **74**, 4631 (1995).
[24] J. H. Macek and S. Yu. Ovchinnikov, Phys. Rev. A **54**, 1 (1996).
[25] A. Erdelyi, W. Magnus, F. Oberhettinger, and F. G. Triocomi, *Higher Transcendental Functions-Volume II* (McGraw-Hill, New York, 1953), p. 75.
[26] P. A. Braun, Rev. Mod. Phys. **65**, 115 (1993).
[27] E. A. Solov'ev, Usp. Fiz. Nauk. **157**, 437 (1989) [Sov. Phys. Usp. **32**, 228 (1989)].
[28] N. F. Mott and H. S. W. Massey, *The Theory of Atomic Collisions*, 3rd ed. (Clarendon, Oxford, 1965), p. 402.
[29] J. H. Macek and S. Y. Ovchinnikov, Phys. Rev. A **50**, 468 (1994).
[30] R. Peterkop and A. Liepinsh, J. Phys. B **14**, 4125 (1981).
[31] A. R. P. Rau, J. Phys. B **9**, L283 (1976).
[32] G. Handke, dissertation, Technische Universität München, Verlag Marie L. Leidorf, Buch am Erlbach (1993).
[33] K. Bartschat and I. Bray, Phys. Rev. A **54**, R1002 (1996). We are indebted to Professor Bartschat for sending us tables of cross sections computed using the CCC and the *R* matrix with pseudostates methods.
[34] M. Abramowitz and I. A. Stegun, *Handbook of Mathematical Functions* (National Bureau of Standards, Washington, D.C., 1964).